

Contents lists available at ScienceDirect

Acta Materialia

journal homepage: www.elsevier.com/locate/actamat



Full length article

Effects of microstructure on the mechanical properties of Ti₂AlC in compression



Rogelio Benitez ^a, Huili Gao ^a, Morgan O'Neal ^a, Peter Lovelace ^a, Gwénaëlle Proust ^b, Miladin Radovic ^{a, c, *}

- ^a Department of Mechanical Engineering, Texas A&M University, College Station, TX 77843, USA
- ^b School of Civil Engineering, University of Sydney, Sydney, NSW 2006, Australia
- ^c Department of Material Science and Engineering, Texas A&M University, College Station, TX 77843, USA

ARTICLE INFO

Article history:
Received 27 November 2016
Received in revised form
25 September 2017
Accepted 6 October 2017
Available online 7 October 2017

Keywords: MAX phases Ti₂AlC Hall-Petch effect Microstructure Compressive strength Non-linear hysteretic

ABSTRACT

This study investigates the effect of microstructure, specifically the grain size and TiAl_x impurity, on the compressive strength and hysteretic behavior of Ti₂AlC at room temperature. Given the plate-like nature of the MAX phase grains, the length and thicknesses of over 100 grains for each microstructure were measured. A Hall-Petch like relationship between compressive strength and the grain length was observed, but not such a relationship was observed with the grain thickness. Results from cyclic compression testing in combination with resonant ultrasound spectroscopy show that room temperature mechanical response of Ti₂AlC can be divided into four stress regions regardless of the variation in grain size and/or amount of impurities. The grain size effect on the transition stresses for stress regions was also investigated. It was found that all transition stresses, between the different stress regions, also follow different Hall-Petch-type relationships.

© 2017 Acta Materialia Inc. Published by Elsevier Ltd. All rights reserved.

1. Introduction

Ti₂AlC belongs to a class of ternary carbides and nitrides, usually referred to as MAX phases, whose unique combination of metallic and ceramic like properties have sparked great interest since the first MAX phase, namely Ti₃SiC₂, was synthesized in bulk [1,2]. In general, MAX phases have high stiffness, strengths, electrical and thermal conductivity combined with low density and hardness, excellent machinability, and thermal shock resistance [3,4]. Out of more than 70 compounds discovered to date, Ti₂AlC is one of the most promising candidate for structural applications at high temperature, especially in air and humid environments, due to its high oxidation resistance provided by a self-forming Al₂O₃ protective layer that is resistant to spalling even during thermal cycling [5-9]. Since Ti₂AlC is one of the most attractive MAX phases for different applications, it is not surprising that numerous studies published to date reported on its mechanical properties. However, a review of those studies shows great variations of its compressive strength at

E-mail address: mradovic@tamu.edu (M. Radovic).

room temperature. In quasi-static loading conditions, its compressive strength spans from the lowest reported value of 393 MPa to the highest one of 1263 MPa (the results of the different studies are summarized in Table 1 [10-22]). At high strain rates, compressive strengths of Ti₂AlC ranging from 517 MPa to 1863 MPa were measured using the Split Hopkinson Pressure Bar (SHPB) technique [22,23]. It is clear from Table 1 that the lowest and highest values reported for the compressive strength of that material correspond to samples with the largest and smallest grain sizes, respectively, indicating a Hall-Petch type relationship. A Hall-Petch type relationship between compressive strength and grain size has been proposed before for some other MAX phases, such as V₂AlC [3], (Ti,Nb)₂AlC [24], and Ti₃(Si,Ge)C₂ [25,26]. However, at first glance, the rest of the compressive strengths values in Table 1 that range from 540 MPa to 910 MPa, do not seem to have a clear dependency on their grain size. The later suggest that some other microstructural factors might contribute to the mechanical response of Ti₂AlC under compressive loading, besides gran size.

The final microstructure of Ti_2AlC depends strongly on its processing route [27]. In general, there are two types of reaction synthesis of Ti_2AlC . The first route uses the binary carbide Al_4C_3 with Ti and C powders as reactants that reaction sinter in the

 $[\]ast$ Corresponding author. Department of Mechanical Engineering, Texas A&M University, College Station, TX 77843, USA.

Table 1Summary of processing conditions and resulting mechanical properties for Ti₂AlC from literature.

Compressive Strength (MPa)	Microstructure		Processing Condition	Reference				
	Grain Length (μm)	Grain Thickness	Impurities Detected	Sintering Method	Temperature	Time hrs		
		(μm)			(°C)		#	
393	100-200	_	_	Hot Press	1600	4	[10]	
540 ± 21	25	_	Al ₂ O ₃ & TiAl _x	Hot Isostatic Press	1300-1400	15-48	[11]	
560	41 ± 12	16 ± 4	None	Hot Press	1450	1	[12]	
655 ± 32	10 ± 2	5 ± 2	None	Hot Press	1350	2	[13]	
670	15	_	Ti ₃ AlC ₂	Hot Press	1400	1	[14]	
865 ± 55	20 ± 10	8 ± 2	None	Hot Isostatic Press	1400	2	[15-18]	
910	_	_	_	_	_	_	[19]	
1037	6		TiAl _x	SHS/PHIP		25 s	[20]	
1057 ± 84	3.05	_	TiAl _x	SHS/PHIP	_	25 s	[21]	
1263	4.2	2.1	TiAl _x Ti ₃ AlC ₂	SPS	1300	15 min	[22]	

1300 °C-1600 °C temperature range. Since aluminum carbide is a very stable compound that slowly reacts with Ti and C, long processing times of 4-48 h is required to produce Ti₂AlC [11]. The second and more widely used approach, as it primarily reduces processing time, is to use elemental powders of Al in combination with Ti, C and/or TiC as reactants. A significant reduction in processing time is achieved using this route because aluminum melts at 660 °C, forming a liquid that promotes fast reaction and sintering. This type of reaction is commonly referred to as solid-liquid reaction and has been shown to produce high purity Ti₂AlC after reaction sintering in as short as 1 h [12,28–31]. Alternately, these same reactants have been used in self-propagating high-temperature synthesis (SHS) to produce high purity Ti₂AlC in the order of seconds [20,21,32-34]. One drawback of using pure aluminum powder as a reactant is that it evaporates during sintering and therefore, its amount in initial powder mixture has to be adjusted to compensate for the aluminum that volatizes during synthesis [30,35,36], or otherwise the final product would have large amount of secondary phases such as TiC or nonstoichiometric TiAlx intermetallic [27,37]. The evaporation rate of aluminum depends on many processing factors, including chamber pressure (vacuum or inert gas), gas purge rates, and heating rates among others, such that tuning the correct initial stoichiometry quickly becomes more an art than a science. In addition, since Ti₂AlC is stable only in very narrow compositional range, the final stoichiometry has to be near perfect to avoid formation of secondary phases [3]. Therefore, when analyzing the spread of compressive strengths in Table 1, the effect of undesired secondary phases should be accounted for, because their eventual presence can also affect the mechanical behavior of Ti₂AlC. Although many sources claim high purity of their samples, their claims are based solely on X-ray diffraction (XRD) results, and are not supported by any other more accurate analysis [12,14,15,18]. This approach could be potentially misleading since small amounts of impurities, especially TiAlx may accumulate in triple grain junctions or as a thin film in grain boundaries, such that their size and amount may be small, and thus undetectable using XRD. In addition, since impurities present in the material are products of incomplete reactions and/or of less than ideal stoichiometry in the final product, they may form with distorted stoichiometry and/or crystal lattice which might result in peak broadening, to such an extent that the peaks might be lost in the XRD background signal.

It is also well established by now that Ti_2AlC , and to further extent other MAX phases, do not behave as typical brittle ceramics before they fail in compression. In other words, their stress-strain behavior is not linear-elastic, but rather non-linear hysteretic resulting in large hysteresis loops when samples are exposed to loading-unloading cycles [15–19,26,38–46]. Therefore, the mechanical energy dissipation during a loading-unloading cycle (W_d)

and the stress at which the first hysteresis loop can be observed (σ_t) are other important parameters that describe the mechanical response of MAX phases. It is well documented that W_d and σ_t in MAX phases also depend on their microstructure, i.e. they are grain size dependent, with coarse grained structures dissipating more energy than fine grained ones. According to the Kinking Nonlinear Elastic (KNE) model [26,38,41,44,47] i.e. the first model proposed to explain hysteretic behavior of MAX phases — this behavior has been attributed to easier incipient kink bands (IKBs) formation in coarse grained structure, as it is described in more details elsewhere [44,47,48].

However, recently other models have been proposed to explain the reversible hysteretic behavior in MAX phases. Poon et al. [19] proposed that the hysteretic behavior of MAX phases can be attributed to the formation of delamination microcracks and friction between crack faces during cyclic loading, which in turn can be also scaled to the grain size. More recently, Jones et al. [43] also challenged the relevance of IKBs formation on the hysteretic behavior and proposed as an alternative another underlying hysteretic mechanism, namely reversible flow or dislocation glide of basal plane dislocations in soft grains, i.e. grains in which the critical resolved shear stress (CRSS) is first reached because of their favorable orientation relative to the direction of applied load. Referred to as the Reversible Flow (RF) model, this proposed model is based on observations of inhomogeneous residual lattice strains that develop during loading of polycrystalline Ti₃SiC₂ in compression and simulation results obtained using an elasto-plastic selfconsistent (ESPC) model [49–51]. Since the RF model proposes that the stress-strain hysteretic behavior in MAX phases can be attributed to reversible glide of basal plane dislocation, both W_d and the onset stress for micro-yielding due to dislocation glide in soft grains should obey a Hall-Petch type dependency on grain size, as it is discussed in more details elsewhere [43]. Most recently, movement of these bulk ripplocations - and not basal dislocations as previously assumed - was proposed as mechanisms responsible for or the fully and spontaneously reversible loops in Ti₃SiC₂ and possibly in other MAX phases [52,53].

In our recent work we reconciled some of those single mechanistic models and proposed that the cyclic compressive behavior of Ti₂AlC can be divided into four stress regions, each with a different dominant underlaying hysteretic mechanism [54]. Analysis of the results obtained from cyclic compression testing of high purity Ti₂AlC in that study, more specifically changes of W_d and irrecoverable strain after first loading (Δ e_{PL}), in combination with results of resonant ultrasound spectroscopy (RUS) and electron backscatter diffraction (EBSD) studies suggested the following stress regions with distinct mechanical responses [54]: (i) Region I at low stress range in which the mechanical response is linear elastic; (II) Region

Table 2Summary of processing conditions, amount and type of impurities, grain sizes and mechanical properties of all samples tested in this study.

Sample	Powder	Sintering Technique	Post Heat	Secondary Phases			Grain Size			Compressive	Strain to
	Source		Treatment	Detected		Length	Thickness	AR	Stress (MPa)	Failure (%)	
			(hr)	XRD	SEM/EDX	Vol % TiAl _x	(µm)	(µm)			
CS-CG	Maxthal 211	PS 1500 °C 4 h	0	TiAl _x ; Ti ₃ AlC ₂ ; Ti ₅ Al ₂ C ₃	TiAl _x ; Ti ₃ AlC ₂ ; Ti ₅ Al ₂ C ₃ ; Al ₂ O ₃	17	22 ± 22	5 ± 2.6	4.4	565 ± 15	1.51 ± 0.03
CP-FG	Maxthal 211	SPS 1300 °C 15 min	0	TiAl _x Ti ₃ AlC ₂	TiAl _x ; Ti ₃ AlC ₂ ; Al ₂ O ₃	7	4.2 ± 2.5	2.1 ± 1	2.1	1263 ± 45	1.15 ± 0.09
RP-FG	RP	SPS 1300v°C 45 min	0	_	TiAl _x ; Al ₂ O ₃	3	6.1 ± 2.8	4.6 ± 2.2	1.4	1040 ± 10	1.25 ± 0.05
RP-MG	RP	SPS 1300 °C 45 min	8	_	TiAl _x ; Al ₂ O ₃	3	13.9 ± 8	7.3 ± 2.4	1.9	820 ± 10	0.99 ± 0.03
RP-CG	RP	SPS 1300 °C 45 min	24	_	TiAl _x ; Al ₂ O ₃	3	17.4 ± 9.7	8.2 ± 2.9	2.2	640 ± 30	1.04 ± 0.20
RP-XCG	RP	SPS 1300 °C 45 min	72	_	TiAl _x ; Al ₂ O ₃	3	44.7 ± 39.2	13.8 ± 7.5	3.2	430 ± 60	0.76 ± 0.03
SC	RP + Ti + Al	SPS 1300 °C 20 min	0	TiAl _x	TiAl _x ; Al ₂ O ₃	17	7.8 ± 2.9	4.3 ± 1.9	1.4	1110 ± 20	1.40 ± 0.08
RS- SPS	Ti + Al + TiC	SPS 1450 °C 15 min	0	_	TiAl _x	5	6.9 ±	$4.5 \pm$	1.5-	1200 ± 55	1.11 ± 0.08

II above micro-yielding stress denoted as $\sigma_{\text{I-II}}$ in which a small stress-strain hysteresis was observed during cyclic loading, in conjunction with a rapid increase in permanent deformation in the first loading-unloading cycle - a behavior attributed to reversible glide in soft grains; (iii) Region III at stresses higher than the microyielding stress denoted as σ_{II-III} in which formation of Low Angle Kink Boundaries (LAKB) most likely gave rise to the observed cyclic hardening and more pronounced hysteretic behavior [55]; and (iv) Region IV at very high stresses exceeding the critical stress denoted as σ_{III-IV} where microcracking appears and attainably affects the observed hysteretic behavior by increasing the total energy dissipated in each loading-unloading cycle. In addition, results reported in that study for two microstructures with different grain sizes, suggested that all transition stresses, namely σ_{I-II} , σ_{II-III} , σ_{III-IV} , and the compressive strength are functions of the grain size. In this work, the effects of microstructure including grain size and TiAl_x intermetallic impurity on the ultimate compressive strength and hysteric behavior of Ti₂AlC at room temperature are investigated in more details. It is, to the best of the authors' knowledge, the first systematic study of the effects of microstructure on the room temperature mechanical properties of Ti₂AlC.

2. Experimental procedure

To produce samples with different grain sizes and various amounts of intermetallic impurities, the samples tested in this study were fabricated using three processing routes, utilizing powders synthesis in-house as well as commercially available powders (MAXthal 211, Sandvik Heating Technology, Sweden). Processing routes for all samples are summarized in Table 2 and briefly described below.

Commercial Sample (CS-CG): commercially available Ti₂AlC (3-ONE-2, Voorhees, NJ) was prepared by cold compaction followed by pressureless sintering of MAXthal 211 powder at 1500 $^{\circ}$ C for 4 h in a vacuum of 10^{-2} torr. Those samples are further denoted as commercial sample - coarse grained or CS-CG.

Commercial Powder (CP-FG): Spark Plasma Sintering¹ (SPS25-10, Thermal Technology LLC, USA) was used to fabricate high density samples from MAXthal 211 commercial powders. In short, the asreceived powders were placed in a graphite die that was later positioned inside the SPS chamber. The samples were heated to 1300 °C at 50 °C min⁻¹ for 15 min under an applied pressure of 100 MPa and then cooled near to room temperature at a rate of 50 °C min⁻¹. Those samples are further denoted as commercial

powder-fine grained or CP-FG.

Reacted Powder (RP): In an effort to produce higher purity Ti₂AlC, a two-step process was employed in which Ti₂AlC powders were synthesized in-house followed by sintering in SPS. For the Ti₂AlC powder synthesis, Ti (99.5%, -325 mesh), Al (99.5%, -325 mesh) and TiC (99.5%, 2 µm) powders, all from Alpha Aesar, USA, were used. The powders were weighed to achieve a molar ratio of Ti:Al:C = 2:1.05:0.95 and mixed by ball milling for 24 h. The mixture was placed in alumina boats and sintered in a high vacuum tube furnace (GSL1600X, MTI Corporation, USA) at a calibrated temperature of 1400 °C under UHP argon. The sintered compact of reacted powder was then drill milled and sieved to obtain -170 mesh Ti₂AlC powder and then processed in SPS to produce high density samples, by sintering for 45 min at 1300 °C. Those samples are further denoted as fine grained or RP-FG. To explore the effect of grain size while maintaining an invariant amount of impurities, samples were further subjected to 8, 24, and 72 h heat treatment at 1400 °C. Those samples are further denoted as medium, coarse and extra-coarse grained, or RP-MG, RP-CG, and RP-XCG, respectively.

Sintered Composite (SC): A set of samples were fabricated in which excess aluminum and titanium powders were added to prereacted in-house Ti₂AlC powders to produce Ti₂AlC samples with a higher amount of TiAl_x with a grain size comparable to the CS-CG sample. Excess Ti and Al were added to result in formation of approximately 17 vol% of TiAl_x. After weighing, Ti, Al and Ti₂AlC powders were mixed by ball milling for 24 h and sintered in SPS at 1300 °C for 20 min at 100 MPa.

Reaction Sintered (RS- SPS): The same powders as in the case of RP samples were mixed to yield Ti:Al:TiC ratio of 1:1.05:0.75 and ball milled for 24 h. The powder mixture was compacted in graphite die and reaction sintered in SPS at 1450 °C for 20 min, as described elsewhere [37].

X-ray diffraction (XRD) spectra (not shown here) for all samples were collected using a diffractometer (D8 Discover, Bruker, USA) with Cu-K α radiation at 40 kV and 40 mA in 8°–80° 2 θ range with a 0.024° step and a rate of 3.5°/min. In addition, the microstructure of the samples was characterized using a field emission scanning electron microscope (SEM, Quanta 600 FEG, FEI, USA) equipped with a back-scattered electron (BSE) detector and an Energy-Dispersive Spectroscopy (EDS) system (Oxford Instruments, UK). The volume percent of intermetallic impurities in the samples was calculated by performing image analysis with Image J software on electron micrographs obtained with the BSE detector. The volume percent of impurities was determined using:

$$Vol_{TiAl}\% = \left(\frac{Area_{TiAl}}{Area_{Total}}\right) * 100 \tag{1}$$

 $^{^{1}}$ Less common but more appropriately referred to as Electric Current Assisted Sintering (ECAS).

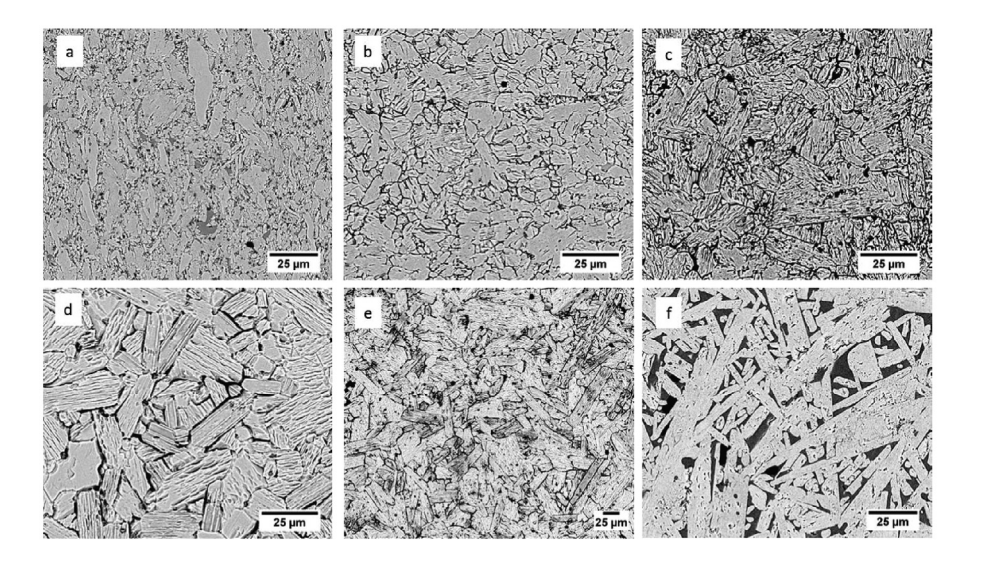


Fig. 1. Selected but typical backscatter electron micrographs of examined samples: (a) etched CP-FG; (b) etched RP-FG; (c) etched RP-MG; (d) etched RP-CG; (e) etched RP-XCG and (f) unetched CS-CG where the dark gray phase between Ti_2AlC grains was identified by EDS as $TiAl_x$.

In this study only titanium intermetallic phases $TiAl_x$ were accounted for because they represented the major impurity phases in all the samples (Table 2). In addition, the length and thickness of more than 100 grains were measured for each processed set of samples from SEM images using Image J software. The density of sintered samples was measured by the alcohol (200 proof ethanol) immersion method based on Archimedes' principle described in more detail elsewhere [56,57]. The relative density (not shown here) was fund to exceed 98% for all processed samples.

Cylindrical samples, 5 mm in diameter and 8 mm in length, were cut by wire electro-discharge machining (Wire-EDM) for quasistatic compression testing. The samples were tested using a servo-hydraulic testing machine (MTS-810, MTS, USA) under a constant crosshead displacement rate chosen to result in a strain rate of $10^{-4}~\rm s^{-1}$. A high temperature axial extensometer (632.59, MTS, USA) was attached to WC spacers placed between sample and pushrods. Since the extensometer was not placed directly on the sample, the strain in the sample was corrected using

$$\varepsilon_{eff} = \frac{GL^*\varepsilon_{ext}}{L_0} \tag{2}$$

where ε_{eff} is the effective strain in the sample, GL is the gauge length of the extensometer (15.24 mm), ε_{ext} is the strain measured by extensometer, and L_0 is the sample's initial length. This simple correction assumes zero contraction of the spacers as well as perfect contact between sample and spacers, so the values of the strains reported are only approximations of the strain magnitudes experienced by the sample and are thereby referred to as effective strains

Cyclic compression testing was perform on all but the SC sample following the procedure outlined in more detail in our previous work [54], whereby cylindrical samples, 9 mm in diameter by 16.5 mm in length were cut by Wire-EDM and tested in compression on a servo-hydraulic testing machine (MTS-810, MTS, USA) at a frequency of 0.5 Hz. Strains were measured with an axial extensometer (632.13E-23, MTS, USA) directly attached to the sample while the sample was loaded and unloaded twice in each testing step to the prescribed maximum load. A preload of 5 MPa was maintained while the stress amplitude was increased for 50 MPa in each testing step to failure. Resonant ultrasound spectroscopy

(RUS) was used to measure the changes in Young's modulus after each testing step as described elsewhere [54] with the goal to determine the onset of its decrease due to microcracking of the samples.

3. Results and discussion

3.1. Microstructure of as-processed samples

Representative BSE micrographs of polished and etched surfaces in Fig. 1a-e illustrate different grain morphologies and sizes in selected as-processed samples. Those and similar micrographs for other samples not shown in Fig. 1a-e were used to measure the length (l) and thickness (t) of more than 100 grains for each sample. The length and thickness were measured separately in this study because of the plate-like nature of MAX phase grains. It is assumed that the length of the grain is equal to the length of the basal planes and that the thickness is equal to grain dimension along the [0001] direction. The arithmetic mean values and standard deviation of land t are listed in Table 2 for all as-processed samples, together with average aspect ratios (AR). Those results show that the grain size ($l \times t$) in the as-processed samples varied from $4.2 \times 2.1 \, \mu \text{m}^2$ to $44.7 \times 13.8 \ \mu m^2$ and that samples with larger grain sizes have, in general, a higher aspect ratio. Note here that the grain size in RP samples increases from 6.1 \times 4.6 μ m² in as-processed sample (RP-FG) to $44.7 \times 13.6 \,\mu\text{m}^2$ in the sample that was heat treated for 72 h after sintering (RP-XCG). In addition, the aspect ratio in those samples increases monotonically with increasing grain size, as it is expected in MAX phases due to their anisotropic grain growth, i.e. faster growth in the direction of basal planes [3]. It is important to note that the grain size variation, measured by the standard deviation, increases with the grain size. The larger the grain size, the higher the probability of finding a few grains much larger than the reported average grain size such that the distribution of grain sizes would be approximated much better with a log-normal distribution.

XRD results (not shown here) did not reveal the presence of any secondary phases in most as-processed samples, Table 2. The only exceptions are CS-CG, CP-FG and SC samples in which different secondary phases, such as nonstoichiometric TiAl_x intermetallic,

Ti₃AlC₂ and Ti₅Al₂C₃ were identified by XRD. Additional analysis of polished but unetched surfaces by BSE and EDS, revealed the presence of small amounts of other phases, identified by EDS to be close to Al₂O₃, TiAl_x, Ti₃AlC₂, and/or Ti₅Al₃C₂ phases even in XRD pure samples, Table 2. Since TiAl_x was identified to be the major non-MAX phase² impurity in most of the samples (note that the amount of Al₂O₃ in all samples was <1–2%), its amount was determined from BSE images of polished and unetched surfaces, similar to the one shown in Fig. 1f, using procedure described earlier. Results of that analysis, listed in Table 2, show that the amount of TiAl_x in processed samples varied between 3 vol% in RP-SPS samples to 17 vol% in CS-CG and SC samples.

3.2. Stress-strain response in quasi-static compression

Selected but typical stress-strain curves in Fig. 2, as well as average values of compressive strengths and strains at failure in Table 2, clearly illustrate large variations in the mechanical responses of samples with different microstructures that were processed using various routes. While at very low stresses (below 100-200 MPa) all samples behave almost identically in a nearly linear-elastic manner, at higher stresses their mechanical behavior is quite different. In the case of the CP-FG samples, which had the smallest grain size, the mechanical behavior in compression was brittle-like with failure at very small strains (<1%). Moreover, all those samples failed catastrophically in a brittle manner by shattering into many small pieces. However, the average compressive strength of 1263 MPa for the CP-FG samples is the highest measured in this study, and, even more, the highest ever reported for Ti₂AlC for quasi-static loading conditions. Another extreme example is shown by samples with very coarse grain structures, namely CS-CG and RP-XCG that have more quasi-ductile behavior and significantly lower compressive strength. These samples usually fracture into two pieces, with typical fracture occurring close to 45° relative to the direction of applied loading, suggesting failure by shear band formation [58,59]. In addition, in the samples with the two largest grain sizes, the two fracture pieces remained weakly attached to each other after completion of testing. The latter is attributed to the effect of crack bridging that was previously observed in coarse grained MAX phases [60]. Note that CS-CG shows the most graceful failure and the largest strains at failure. for the reasons that are discussed in more detail at the end of this section. The mechanical response of all other samples (Fig. 2 and Table 2) lies in between those two extremes (i.e. very fine and very coarse grained structures) and they show some moderate softening and pseudo-ductility before final graceful failure.

The average compressive strengths of all the samples tested in this study are plotted in Fig. 3 as a function $1/\sqrt{l}$ and $1/\sqrt{t}$ where l and t are the average grain length and thickness, respectively, from Table 2. For comparison, previously reported values of compressive strengths listed in Table 1 are also plotted in Fig. 3, only if the average grain length and thickness were reported in the original work. Linear regression fitting of the results obtained in this study and plotted in Fig. 3 has been carried out using a Hall-Petch type of relationship between compressive strength (σ_f) and the average grain length (l):

$$\sigma_f = \sigma_0 + k_f * l^{-1/2} \tag{3}$$

For our results it gives Hall-Petch constants $\sigma_0=70.5$ MPa and $k_f=2633$ MPa/ $\sqrt{\mu}m$ with $R^2=0.91$. However, no correlation was

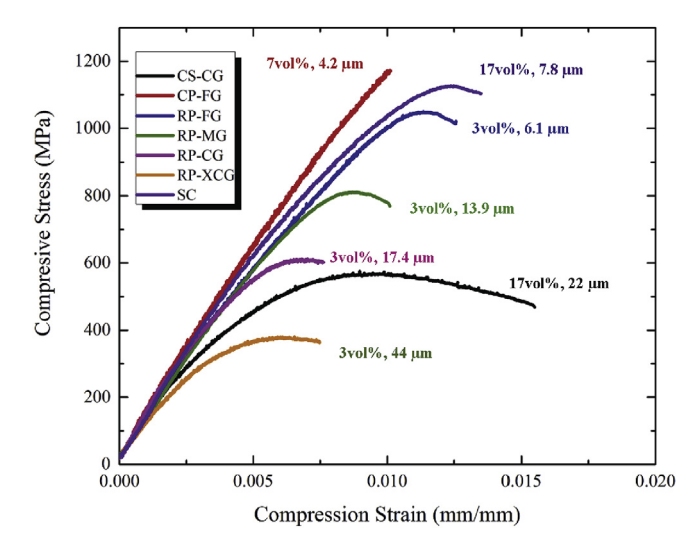


Fig. 2. Selected but typical stress-strain curves obtained in quasi-static loading to failure. Numbers next to the each stress-strain curve show the volume percent of $TiAl_x$ impurities and grain length.

found between the compressive strength and the average grain thickness, t. Fitting results in Fig. 3b using a similar Hall-Patch relationship, i.e. $\sigma_f = \sigma_0 + k_f * t^{-1/2}$ yields very low value of $R^2 = 0.61$, suggesting that there is no correlation between the compressive strength and the thickness of the grains. The possible underlying failure mechanisms responsible for the observed Hall-Petch type relationship between compressive strengths and grain length in Ti₂AlC are discussed in more detail in the next section, after the analysis of the results of cyclic loading.

At the end of this section, the effect of TiAl_x impurities on the mechanical behavior of Ti₂AlC in compression has to be addressed in more detail. Results in Fig. 3 together with the good fitting results using Hall-Petch type equations, clearly show that the amount of TiAl_x impurities (up to 17 vol%) does not affect significantly the compressive strength. However, the presence of a higher amount of TiAl_x contributes to larger strains to failure. For example, the CS-CG sample and SC sample both with high (~17 vol%) amount of TiAl_x exhibit the higher strains to failure. Note that TiAlx is less stiff (E = 176-184 GPa, G = 70-76 GPa [61]) and rather ductile [62] when compared to Ti₂AlC and thus it has the potential to enhance the strain to failure by deforming plastically more than MAX phase. Moreover, it has been shown that cracks do not propagate through TiAl_x when present in other MAX phases [63]. It is important to note that this response is not observed in the CP-FG sample, probably due to its fine grain size and the fact that TiAl_x in these samples is limited to isolated pools thereby hindering its ability to shield the damage.

3.3. Cyclic compression testing

In general, the Hall-Petch relationship, such that shown in Eq. (3), is usually used to describe the relationship between: (i) yield strength and grain size in dislocation-based ductile materials when yielding is controlled by dislocation glide in multiple slip systems and hindered by grain boundaries; and (ii) strength and grain size in brittle materials with limited number of slip systems and/or high CRSSs when strength is controlled by microcracks having size close to the grain size [64–67]. However, in MAX phases, taking a middle ground between ductile metals and brittle ceramics, the nature of this relationship is much more complex. We have recently showed [54], that mechanical behavior of Ti₂AlC is characterized by three micro-yielding stresses, namely $\sigma_{\text{I-II}}$, $\sigma_{\text{II-III}}$, and $\sigma_{\text{III-IV}}$, as it is briefly

 $^{^2}$ Ti $_3\text{AlC}_2$ and Ti $_5\text{Al}_3\text{C}_2$ also belongs to the family of MAX phases and cannot be easily distinguished from Ti $_2\text{AlC}$ on BSE images.

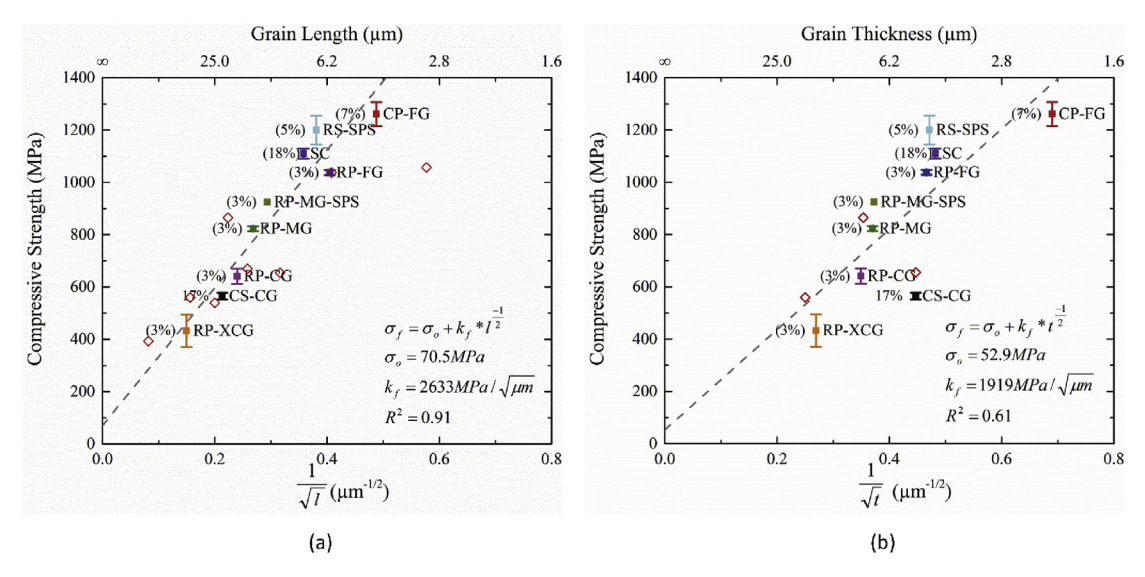


Fig. 3. Average compressive strength of Ti_2AIC plotted to show a possible linear relationship according to the Hall-Petch manner effect as a function of $(a)1/\sqrt{t}$, where l is the average grain length and $(b)1/\sqrt{t}$, where l is the average grain thickness. Error bars indicate standard deviation in compressive strengths. The dashed lines represent the best fitting linear relationship for the results obtained in this study. Numbers in parenthesis denote vol% of $TiAl_x$ impurities in each sample. For comparison, some reference values published before and listed in Table 1 are also plotted as open red symbols (\diamondsuit). (For interpretation of the references to colour in this figure legend, the reader is referred to the web version of this article.)

described in the introduction of this paper.

Following the very same procedure used in our previous work [54], selected samples from Table 2, namely CS-CG, CP-FG, RP-FG, RP-MG, RP-CG, RP-XCG, were exposed to series of cyclic loading testing in compression complemented by elastic modulus measurements by RUS. Results of this exercise are summarized for selected samples in Fig. 4 showing the changes of energy dissipated per each loading cycle (W_d), the opening of the first loop or irrecoverable strain ($\Delta\sigma_{PL}$) after each subsequent loading to higher

stress, and the relative Young's modulus (defined as the ratio of Young's modulus measured after cycling to the designated stress to Young's modulus of the as-processed sample) with σ^2 , where σ is maximum stress in each loading cycle. Those results were used to determine the following characteristic stresses:

• σ_{I-II} as the onset of Region II that is characterized by small hysteresis loops and a steep increase in $\Delta\sigma_{PL}$ with σ^2 ;

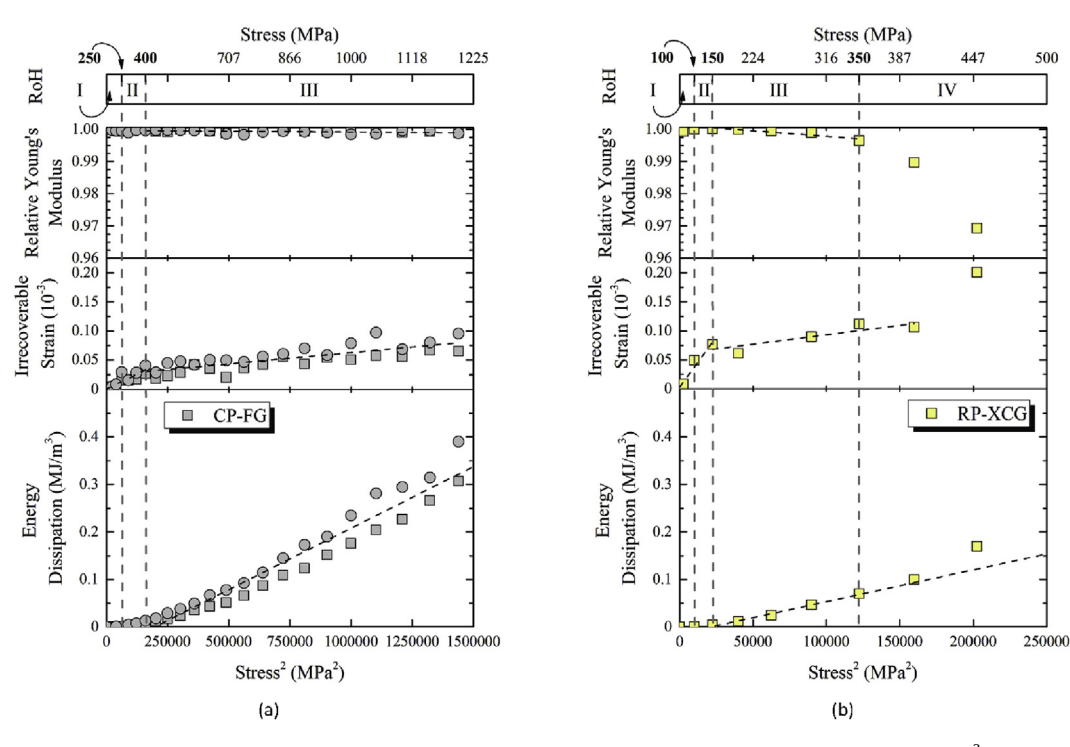


Fig. 4. Selected but typical results of cyclic testing in compression of (a) sample CP-FG and (b) sample RP-XCG. Bottom plots: W_d as a function of σ^2 ; Middle plots: $\Delta \sigma_{PL}$ as a function of σ^2 ; Top plots: Relative Young's modulus as a function of σ^2 . Topmost scales indicate stress regions with different mechanical behavior observed in this study, while vertical dash lines denote micro-yielding.

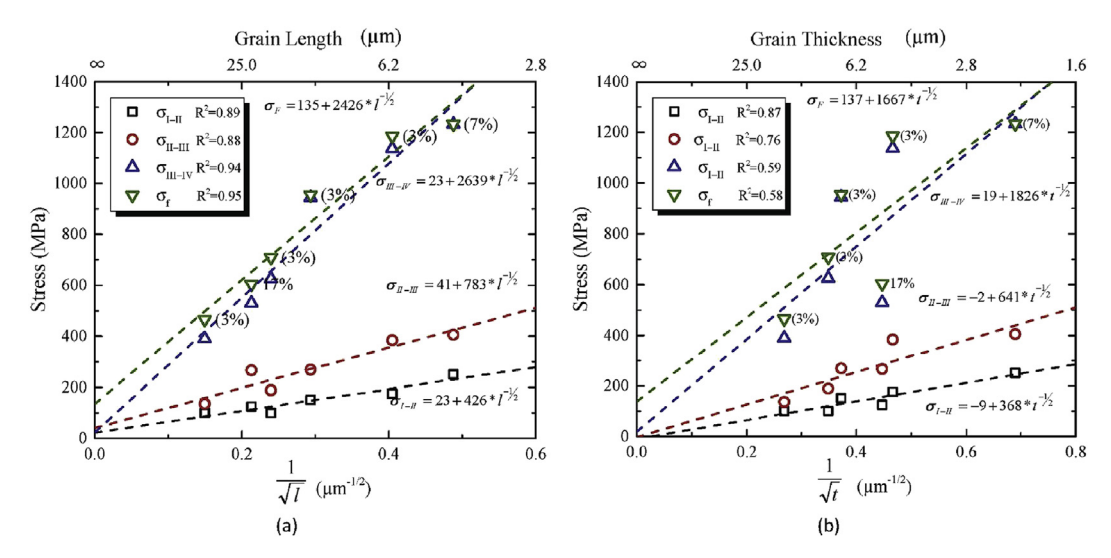


Fig. 5. Characteristic stresses for the stress Regions as a function of the inverse square root of (a) the grain length and (b) the grain thickness. Corresponding vol% of TiAl_x in each sample is labeled next to each data point.

- σ_{II-III} as the onset of Region III in which W_d scales linearly with σ^2 as predicted earlier [26,38,44], while cyclic hardening causes a much gradual increase in $\Delta\epsilon_{PL}$ with σ^2 than in Region III when compared to Region II;
- σ_{III-IV} as onset of Region III characterized by an elastic modulus drop larger than 0.2% with σ^2 as a result of microcracking and a pronounced upward deviation of W_d from the predict linear dependence with σ^2 ;
- \bullet σ_f as the maximum compressive stress after series of cyclic loading.

The four characteristic stresses σ_{l-ll} , σ_{ll-lll} , σ_{ll-lll} and σ_t , for all samples in this study, are plotted as a function of $1/\sqrt{l}$ and $1/\sqrt{t}$ in Fig. 5, to explore if they yield Hall-Petch type relationships. Note that characteristic stresses plotted in Fig. 5 were calculated as average values determined from testing two samples from each set of specimens with different microstructure. In addition, the results of linear regression fitting assuming Hall-Patch type relationships are denoted by dashed lines in Fig. 5, together with corresponding fitting equations and R^2 values. Those results clearly indicate that all the characteristic stresses plotted as a function of grain length in Fig. 5a obey a Hall-Petch relationship with R^2 values exceeding 0.88. However, it seems that only σ_{l-ll} and σ_{ll-lll} show a Hall-Petch type dependence on grain thickness as indicated by high R^2 values in Fig. 5b. Once again, σ_{lll-lV} and σ_f that correspond to onset of microcracking and failure, do not scale with grain thickness.

As it was discussed in more details in our previous paper [54], σ_{I-II} denotes the onset of plastic flow in soft grains most likely by dislocation glide in basal planes. This is accommodated by the development of elastic residual stresses in hard grains in a similar way as it is proposed by the RF model [43] and demonstrated in neutron diffraction studies [55,68]. Because basal plane dislocations in soft grains pile up against grain boundaries with hard grains, and since the size of the mean free path on basal planes in MAX phases is proportional with the length of the grain, it is reasonable to assume, following original works of Hall and Patch [65,69–71], that the micro-yielding stress σ_{I-II} in polycrystalline Ti_2AIC can be expressed as:

$$\sigma_{I-II} \approx M \cdot \tau_{HP} = M \cdot \left(\tau_{PN} + k_{I-II} * l^{-1/2}\right) = \sigma_{I-II}^0 + k'_{I-II} * l^{-1/2}$$
 (4)

where M is Taylor factor, τ_{PN} is Peierls-Nabarro stress (assumed here to be equal to the CRSS for slip in basal plane), k_{I-II} , k'_{I-II} and σ^0_{I-II} are constants, and the measured grain length (I) is assumed to be equal to diameter (d) of plate-like grain. Since the best fitting results yield $\sigma^0_{I-II}=23$ MPa, it can be shown that $\tau_{PN}=CRSS=7.7$ MPa assuming M=3 for polycrystalline material with a random distribution of crystallographic orientations. Note that the CRSS value found here is much lower than that of ~24 MPa estimated for Ti₂AlC using the KNE model [26], or that of ~36 MPa measured during the compressive testing of Ti₃SiC₂ quasi-single crystals [58]. Since the constant k'_{I-II} can be expressed as [64]:

$$k'_{l-II} = M \cdot \sqrt{\frac{2Gb\tau_c}{k\pi}},\tag{5}$$

where G and b are the shear modulus and Burgers vector, respectively, k is a constant equal to 1 for screw and $(1-\nu)$ for edge dislocations, ν is the Poisson's ratio, and τ_c is the effective stress at the head of the pile-up acting on the grain boundary. Since $k'_{I-II}=426~\text{MPa}/\sqrt{\mu m}, \tau_c$ is equal to 864 MPa for screw and 717 MPa edge dislocations according to Eq. (5), assuming M=3, G=120~GPa, $b=3.05\times10^{-4}~\text{µm}$ and $\nu=0.17$ [3]. Note that those values are well below the maximum theoretical stress for shear deformation on the basal plane in the a-direction, $(0001)[1\overline{2}10]$, which is $\sim 10~\text{GPa}$ [80]. Therefore, the effective stress at the head of the pile-up is insufficient to cause delamination by shear in basal planes. Furthermore, the number of dislocations in the pile-ups can be calculated as

$$n = \frac{\pi d\tau_C}{2Gb}. (6)$$

For calculated values of τ_c [64] this number is equal to 371 for screw and 307 for edge dislocations assuming a grain length of 10 μ m. Furthermore, those numbers yield reasonable values for the dislocation densities ($\rho_{\rm dis}$) in soft grains, 9.5 \times 10¹² m/m³ and 7.9 \times 10¹² m/m³ for screw and edge dislocations, respectively, if the length of those dislocations is equal to the grain length l in soft grains having size of 10 \times 5 μ m². It also follows that the average distance between edge or screw dislocations in the pile ups yields reasonable values of 27–32.6 nm, or approximately 88 b to 107 b, if the length of the dislocation pile up is equal to that of the grain

length (10 $\mu m)$, and if all dislocations are arranged in the single pile up.

The micro-yielding stress $\sigma_{\text{II-III}}$ denotes the onset of Region III [54], in which geometrically necessary dislocations (GND) are generated in all grains, including those with hard orientation, to accommodate basal slip in soft grains, as it is proposed elsewhere [72,73]. In other words, the plastic flow of soft grains cannot be accommodated anymore only by elastic deformation of the grains in which dislocations cannot glide on basal planes. Although, all the details about the formation of GND in this region are not completely clear at this moment, previous Electron-Backscatter Diffraction (EBSD) and neutron diffraction studies [54,55] show that most of these GND arrange in DW or LAKB. Assuming that those dislocation form as proposed in the kinking model originally developed by Orowan [74] and Frank and Stoch's [75], and in the KNE model for the MAX phases [38,42,45,76], relationship between stress and grain size in this region can be expressed as:

$$\sigma_{II-III} \approx M \cdot \tau_{FS} = M \cdot \left(k_{II-III} * t^{-1/2} \right)$$

$$= M \cdot \sqrt{\frac{4G^2 b \gamma_c}{\pi^2} ln \left(\frac{b}{\gamma_c w} \right)} \cdot t^{-1/2} = k'_{II-III} \cdot t^{-1/2}$$
(7)

where τ_{ES} is the critical stress to nucleate kinks [75], γ_c is the critical kinking angle, w is the dislocation core width, k_{II-III} and k'_{II-III} are constants, and other symbols have their usual meaning. Note that Eq. (7) is derived assuming that the IKB length (2α) is equal to the grain thickness, as it is done in the KNE model [38,42,45,76], and thus σ_{II-III} should be a function of t, and not l as in Region II. Following the KNE model, the critical kinking angle in Eq. (7) can be calculated to be $\gamma_c \approx \frac{3\sqrt{3}(1-v)}{8\pi e} \left(\frac{b}{w}\right) = 0.013 \ rad$ assuming $w = 5 \cdot b$ [26]. For that critical angle and M = 3, k'_{II-III} in Eq. (7) yields a value of 737 MPa $\sqrt{\mu m}$, which is in reasonably good agreement with the slope of 641 MPa $\sqrt{\mu m}$ obtained by fitting the data for σ_{II-III} vs. $t^{-1/2}$ in Fig. 5b, i.e. it is only 13% higher than experimentally obtained value. Also note that fitting of those results in negligibly small intercept stress of -1.8 MPa at $t^{-1/2} = 0$, that could be approximated to be zero within the error margin. The latter is also in good agreement with the model depicted in Eq. (7).

At stresses exceeding the transition stress σ_{III-IV} , stress concentration due to dislocation pile-ups at grain boundaries or formation of GND leads to the formation of Zener-Stroh type cracks [77–79]. The later results in the sudden drop of relative elastic modulus and contributes to the energy dissipated in each cycle, as discussed in more detail in our previous study [54]. Following the treatment given by Davidge [80], the stress to open the cracks at the grain boundary can be expressed in the form of a Hall-Petch relationship as:

$$\sigma_{III-IV} \approx M \cdot \tau_{III-IV} = M \cdot \left(\tau_{PN} + k_{III-IV} * l^{-1/2}\right)$$

$$= \sigma_{III-IV}^{0} + k'_{IV-II} * l^{-1/2}$$
(8)

where k_{III-IV} and k'_{I-II} are constants, and the measured grain length (l) is again assumed to be equal to grain diameter (d). This can be further expressed as:

$$k'_{III-IV} = M \cdot \sqrt{\frac{E \cdot b \cdot \sigma_{th}}{2(1+\nu)}} \tag{9}$$

where σ_{th} is the theoretical tensile strength and E is the Young's

modulus of 277 GPa. Eqs. (8) and (9) were derived assuming that the failure stress is a result of stress concentration caused by edge dislocation pile-up at a grain boundary, and that when such pile-up (under stress) produces a tensile stress equal to or greater than the theoretical fracture strength, σ_{th} , then fracture occurs [80]. Note that expressing stress as a function of l in Eq. (8), it is assumed that dislocations can pile-up only along basal planes and that their length scales with grain length. Since $\sigma_{III-IV}^0=23$ MPa from fitting results in Fig. 5a, τ_{PN} can be calculated to be 7.6 MPa from Eq. (7) assuming M = 3. This value is in good agreement with a τ_{PN} of 7.7 MPa that was obtained from the Hall-Petch assumption for the σ_{I-II} micro-yielding stress using Eq. (4). In addition, the best fitting procedure for σ_{III-IV} stresses plotted as a function of $l^{-1/2}$ in Fig. 5a, gives a value of $k'_{III-IV} = 2639 \ MPa \sqrt{\mu m}$. For this value of k'_{III-IV} , M = 3 and E = 277 GPa for Ti_2AlC [81], Eq. (9) gives $\sigma_{th} \approx 20$ GPa which is reasonably close to the ideal (theoretical) tensile strength of basal planes of 25 GPa calculated using ab initio approach for cleavage along basal planes (i.e. delamination) [82].

Fig. 5a also shows that fracture stress σ_t obtained after cyclic loading testing in compression is just slightly higher than that of σ_{III-IV} , suggesting that once microcracks form in the stress Region III, they propagate quite rapidly with increasing stress resulting in final failure. Note here that the constants σ_0 and k_f in Fig. 5a that were determined by fitting the σ_t vs. $l^{-1/2}$ data from cyclic compressive testing using a Hall-Petch type equation (Eq. (3), yield values close to those given in Fig. 3 for quasi-static testing. This suggests that the loading history does not affect significantly the strength of Ti₂AlC, and even more importantly confirms once again that microcracks most likely do not form and propagate during cyclic loading to stresses below σ_{III-IV} .

The excellent fitting of results in Fig. 5 has been achieved using different Hall-Petch like relationships for micro-yielding stresses as it is indicated by high $\rm R^2$ values, $\rm ^3$ regardless of the fact that the two samples contained relatively large amounts of $\rm TiAl_x$ impurities, namely 7 and 17 vol%. This indicates that the presence of $\rm TiAl_x$ does not significantly affects the values of either micro-yielding stresses or compressive strength. The latter does not mean that $\rm TiAl_x$ does not affect hysteretic behavior of $\rm Ti_2AlC$.

Fig. 6 clearly shows that both opening of the first loop ($\Delta \varepsilon_{Pl}$) and the area of subsequent hysteresis loops (i.e. W_d) increase with the grain size, which is in good agreement with previous results and our current understanding of underlying hysteric mechanisms in MAX phases. However, this figure also illustrates that TiAlx impurities have a significant effect on $\Delta \epsilon_{Pl}$ and W_d . For example, sample CS-CG containing 17 vol% of TiAl_x has a significantly smaller grain size that sample RP-XCG containing only 3 vol% of TiAl_x, yet it has larger opening of the first loop and dissipates significantly much more energy per cycle (Fig. 6). Analysis of the results such as those shown in Fig. 4 for all the samples tested here, 4 yields similar conclusion. This finding is in good agreement with previously published studies on the hysteretic behavior of MAX phase – metal composites, such as Ti₂AlC-Mg [15,16,18] and Ti₃SiC₂-NiTi [46] showing that significant improvements in dissipated energy per loading cycle can be achieved by addition of metallic phases to MAX phases. Although this observation is not fully understood at this moment, it is reasonable to conclude here that the addition of less stiff and more ductile phases results in higher irrecoverable and recoverable strains during loading, and thus larger hysteresis loops

 $^{^3}$ the only exception are for the plots of σ_{III-IV} and $\sigma_{\rm t}$ vs $t^{-1/2}$ in Fig. 5b for the reasons that were discussed in more detail earlier.

⁴ Note that only some typical but selected results are highlighted in Fig. 4 because of limited space.

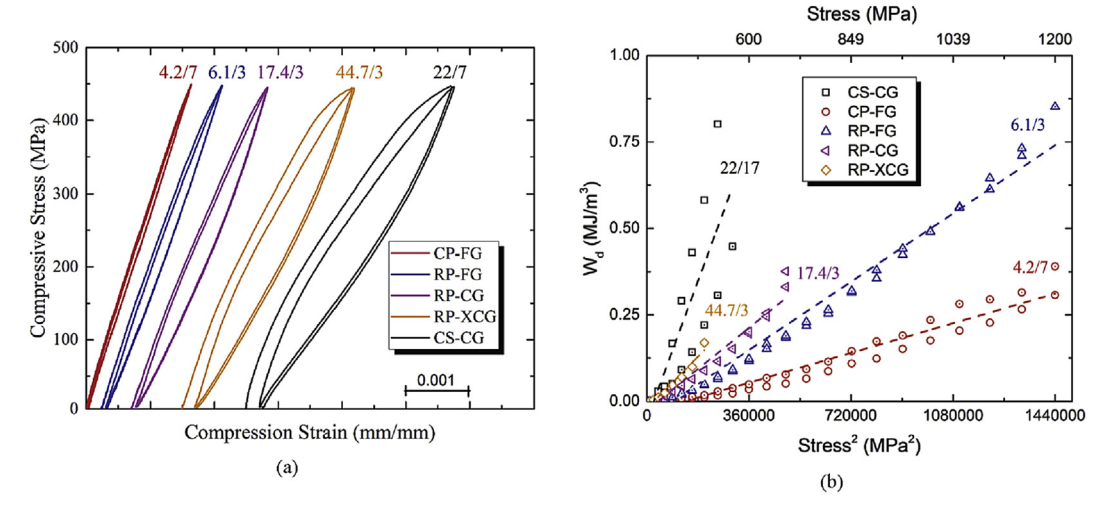


Fig. 6. (a) Selected but typical cyclic stress-strain response for samples with different microstructures loaded to a maximum stress of 450 MPa; (b) W_d vs σ^2 plot with linear regression fitting for samples with different microstructures. Labels on both plots show grain length in $\mu m/vol\%$ of TiAl_x for the different samples.

when compared to pure MAX phase.

4. Summary and conclusions

 ${
m Ti}_2{
m AlC}$ samples with a wide range of different microstructures, i.e. different grain sizes and amounts of ${
m Ti}{
m Al}_{
m x}$ impurities, were tested in compression at room temperature. It was found that the room temperature cohesive strength scales with $l^{-1/2}$, where l is grain length, obeying a Hall-Petch type relationship. However, no correlation was found between compressive strength and grain thickness. Coarse grain structures and the presence of well dispersed ${
m Ti}{
m Al}_{
m x}$ phase were found to enhance the strain to failure and modify the failure mode to a less catastrophic one.

This work also confirms that stress-strain hysteresis in Ti₂AlC can be divided into four stress Regions, each presenting a distinct underlying mechanism, that show different dependence on grain size. The results presented here show that the magnitude of the micro-yielding stress σ_{II-III} , separating Region I of linear elasticity from Region II with hysteretic stress strain behavior, depends on the grain length as it is expected assuming a classical Hall-Patch relationship. This stress marks the onset of basal plane dislocation glide in soft grains, i.e. grains that are favorably oriented for easy slip relative to the direction of the applied load. The microyielding stress $\sigma_{\text{II-III}}$, separating the stress Regions II and III, which display greatly different hysteretic behaviors, shows a linear increase with $t^{-1/2}$, where t is average thickness of the grains. The results of the analysis provided herein suggest that at stresses exceeding $\sigma_{\text{II-III}}$, geometrically necessary dislocations form in all the grains, including those with hard orientation, to accommodate initial plastic flow in soft grains. The assumption regarding the creation of these dislocations made in the kinking model proposed originally by Orowan [74] and Frank and Stroh [75], and later in the KNE model by Barsoum [15,26,38,41,44] to explain hysteretic behavior of MAX phases, are in very good agreement with the experimentally determined change in the value of σ_{II-III} with the grain size. At even higher stresses exceeding the transition stress σ_{III-IV} a reasonably good agreement between observed changes in the value of σ_{III-IV} with the grain length and the models based on formation of Zener-Stroh crack is reached, suggesting that this onset stress of Region III is the stress at which microcracking starts. This finding is in good agreement with previous results [54] that show a significant drop in elastic modulus within Region III as a result of damage accumulation. Last but not least, a critical resolve shear stress of ~8 MPa was determined from two different Hall-Petch type relationships independently, that relating $\sigma_{II\text{-}III}$ and $\sigma_{III\text{-}IV}$ to the grain length.

These results clearly showed that the amount of the $TiAl_x$, a common impurity in Ti_2AlC , does not affect significantly the magnitude of the micro-yielding stresses σ_{I-II} , σ_{II-III} and $\sigma_{III-IIV}$, up to amount of at least 17 vol%. However, larger amounts of $TiAl_x$ where found to result in higher values of irrecoverable strain after microyielding and much larger stress-strain hysteresis loops.

Acknowledgements

This work was supported by National Science Foundation Division of Civil, Mechanical, and Manufacturing Innovation (NSF-CMMI) under grants 1233792 and 1729350, and Division of Materials Research under grant 1410983.

References

- [1] M. Radovic, M.W. Barsoum, MAX phases: bridging the gap between metals and ceramics, Am. Ceram. Soc. Bull. 92 (3) (2013) 20–27.
- [2] M.W. Barsoum, T. El-Raghy, Synthesis and characterization of a remarkable ceramic: Ti3SiC2, J. Am. Ceram. Soc. 79 (7) (1996) 1953–1956.
- [3] M.W. Barsoum, MAX Phases: Properties of Machinable Ternary Carbides and Nitrides, Wiley-VCH Verlag GmbH & Co. Weinheim. Germany. 2013.
- [4] M.W. Barsoum, M. Radovic, Elastic and mechanical properties of the MAX phases, Annu. Rev. Mater. Res. 41 (2011) 195–227.
- [5] S. Basu, N. Obando, A. Gowdy, I. Karaman, M. Radovic, Long-term oxidation of Ti₂AlC in air and water vapor at 1000-1300°C temperature range, J. Electrochem. Soc. 159 (2) (2012) C90–C96.
- [6] X.H. Wang, Y.C. Zhou, High-temperature oxidation behavior of $\rm Ti_2AlC$ in air, Oxid. Metals 59 (3–4) (2003) 303–320.
- [7] J.W. Byeon, J. Liu, M. Hopkins, W. Fischer, N. Garimella, K.B. Park, M.P. Brady, M. Radovic, T. El-Raghy, Y.H. Sohn, Microstructure and residual stress of alumina scale formed on Ti2AlC at high temperature in air, Oxid. Metals 68 (1–2) (2007) 97–111.
- [8] M. Sundberg, G. Malmqvist, A. Magnusson, T. El-Raghy, Alumina forming high temperature silicides and carbides, Ceram. Int. 30 (7) (2004) 1899–1904.
- [9] D.J. Tallman, B. Anasori, M.W. Barsoum, A critical review of the oxidation of Ti₂AlC, Ti₃AlC₂ and Cr₂AlC in air, Mater. Res. Lett. 1 (3) (2013) 115–125.
- [10] M.W. Barsoum, D. Brodkin, T. El-Raghy, Layered machinable ceramics for high temperature applications, Scr. Mater. 36 (5) (1997) 535–541.
- [11] M.W. Barsoum, M. Ali, T. El-Raghy, Processing and characterization of Ti2AlC, Ti2AlN, and Ti2AlC_{0.5}N_{0.5}, Metallurgical Mater. Trans. A 31 (7) (2000) 1857—1865.
- [12] F.L. Meng, Y.C. Zhou, J.Y. Wang, Strengthening of Ti_2AlC by substituting Ti with V, Scr. Mater. 53 (12) (2005) 1369–1372.
- [13] J. Zhu, R. Pan, Synthesis and mechanical properties of (Ti, Mo)2AlC/Al 203 composite by a reaction hot pressing method, Ceram. Int. 39 (5) (2013)

- 5609-5613.
- [14] P. Wang, B.-C. Mei, X.-l. Hong, W.-B. Zhou, Synthesis of Ti₂AlC by hot pressing and its mechanical and electrical properties, Trans. Nonferrous Metals Soc. China 17 (5) (2007) 1001–1004.
- [15] S. Amini, M.W. Barsoum, On the effect of texture on the mechanical and damping properties of nanocrystalline Mg-matrix composites reinforced with MAX phases, Mater. Sci. Eng. A 527 (16–17) (2010) 3707–3718.
- [16] B. Anasori, S. Amini, V. Presser, M.W. Barsoum, Nanocrystalline Mg-matrix composites with ultrahigh damping properties, Magnes. Technol. (2011) 463–468
- [17] A. Kontsos, T. Loutas, V. Kostopoulos, K. Hazeli, B. Anasori, M.W. Barsoum, Nanocrystalline Mg-MAX composites: mechanical behavior characterization via acoustic emission monitoring, Acta Mater. 59 (14) (2011) 5716–5727.
- [18] S. Amini, C. Ni, M.W. Barsoum, Processing, microstructural characterization and mechanical properties of a Ti₂AlC/nanocrystalline Mg-matrix composite, Compos. Sci. Technol. 69 (3–4) (2009) 414–420.
- [19] B. Poon, L. Ponson, J. Zhao, G. Ravichandran, Damage accumulation and hysteretic behavior of MAX phase materials, J. Mech. Phys. Solids 59 (10) (2011) 2238–2257
- [20] Y. Bai, X. He, Y. Li, C. Zhu, S. Zhang, Rapid synthesis of bulk Ti₂AlC by self-propagating high temperature combustion synthesis with a pseudo-hot isostatic pressing process, J. Mater. Res. 24 (8) (2009) 2528–2535.
- [21] Y. Bai, X. He, R. Wang, Y. Sun, C. Zhu, S. Wang, G. Chen, High temperature physical and mechanical properties of large-scale Ti₂AlC bulk synthesized by self-propagating high temperature combustion synthesis with pseudo hot isostatic pressing, J. Eur. Ceram. Soc. 33 (13–14) (2013) 2435–2445.
- [22] P.N. Parrikar, R. Benitez, H. Gao, M. Radovic, A. Shukla, Mechanical response of fine grained Ti2AlC under extreme thermo-mechanical loading conditions, Mater. Sci. Eng. A 658 (2016) 176–184.
- [23] R. Bhattacharya, R. Benitez, M. Radovic, N.C. Goulbourne, High strain-rate response and deformation mechanisms in polycrystalline Ti2AlC, Mater. Sci. Eng. A 598 (2014) 319–326.
- [24] I. Salama, T. El-Raghy, M.W. Barsoum, Synthesis and mechanical properties of Nb₂AlC and (Ti,Nb)₂AlC, J. Alloys Compd. 347 (1–2) (2002) 271–278.
- [25] A. Ganguly, T. Zhen, M.W. Barsoum, Synthesis and mechanical properties of Ti_3GeC_2 and $Ti_3(Si_xGe_{1-x})C_2$ (x=0.5,0.75) solid solutions, J. Alloys Compd. 376 (1–2) (2004) 287–295.
- [26] A.G. Zhou, M.W. Barsoum, Kinking nonlinear elastic deformation of Ti_3AlC_2 , Ti_2AlC , $Ti_3Al(C_{0.5},N_{0.5})_2$ and $Ti_2Al(C_{0.5},N_{0.5})$, J. Alloys Compd. 498 (1) (2010) 62–70
- [27] W. Yu, V. Gauthier-Brunet, T. Cabioc'H, S. Dubois, Synthesis and microstructural characterization of substoichiometric Ti₂Al(C_xN_y) solid solutions and related Ti₂AlC_x and Ti₂AlN end-members, J. Am. Ceram. Soc. 97 (7) (2014) 2308–2313.
- [28] Z.J. Lin, M.J. Zhuo, Y.C. Zhou, M.S. Li, J.Y. Wang, Microstructural characterization of layered ternary Ti₂AlC, Acta Mater. 54 (4) (2006) 1009–1015.
- [29] P. Wang, B. Mei, X. Hong, J. Zhu, W. Zhou, Fabrication of Ti₂AlC by spark plasma sintering from elemental powders and thermodynamics analysis of Ti-Al-C system, J. Wuhan Univ. Technol. Mater. Sci. Ed. 22 (2) (2007) 325–328.
- [30] B. Mei, W. Zhou, J. Zhu, X. Hong, Synthesis of high-purity Ti₂AlC by spark plasma sintering (SPS) of the elemental powders, J. Mater. Sci. 39 (4) (2004) 1471–1472.
- [31] W.B. Zhou, B.C. Mei, J.Q. Zhu, X.L. Hong, Rapid synthesis of Ti₂AlC by spark plasma sintering technique, Mater. Lett. 59 (1) (2005) 131–134.
- [32] A. Zhou, C.A. Wang, Z. Ge, L. Wu, Preparation of Ti₃AlC₂ and Ti₂AlC by self-propagating high-temperature synthesis, J. Mater. Sci. Lett. 20 (21) (2001) 1971–1973.
- [33] Y. Bai, X. He, C. Zhu, G. Chen, Microstructures, electrical, thermal, and mechanical properties of bulk Ti 2 AlC synthesized by self-propagating high-temperature combustion synthesis with pseudo hot isostatic pressing, J. Am. Ceram. Soc. 95 (1) (2012) 358–364.
- [34] Y. Bai, H. Zhang, X. He, C. Zhu, R. Wang, Y. Sun, G. Chen, P. Xiao, Growth morphology and microstructural characterization of nonstoichiometric Ti₂AlC bulk synthesized by self-propagating high temperature combustion synthesis with pseudo hot isostatic pressing, Int. J. Refract. Metals Hard Mater. 45 (0) (2014) 58–63.
- [35] H.J. Yang, Y.T. Pei, J.C. Rao, J.T.M. De Hosson, S.B. Li, G.M. Song, High temperature healing of Ti2_AIC: on the origin of inhomogeneous oxide scale, Scr. Mater. 65 (2) (2011) 135–138.
- [36] G.M. Song, S.B. Li, C.X. Zhao, W.G. Sloof, S. van der Zwaag, Y.T. Pei, J. De Hosson, Ultra-high temperature ablation behavior of Ti₂AlC ceramics under an oxyacetylene flame, J. Eur. Ceram. Soc. 31 (5) (2011) 855–862.
- [37] A. Talapatra, T. Duong, W. Son, H. Gao, M. Radovic, R. Arroyave, High-throughput combinatorial study of the effect of M site alloying on the solid solution behavior of M₂AlC MAX phases, Phys. Rev. B 94 (10) (2016) 104106.
- [38] A.G. Zhou, M.W. Barsoum, S. Basu, S.R. Kalidindi, T. El-Raghy, Incipient and regular kink bands in fully dense and 10 vol.% porous Ti₂AlC, Acta Mater. 54 (6) (2006) 1631–1639.
- [39] P. Finkel, A.G. Zhou, S. Basu, O. Yeheskel, M.W. Barsoum, On the observation of acousto-elastic hysteresis in kinking nonlinear elastic solids, AIP Conf. Proc. (2009) 231–237.
- [40] A. Zhou, M.W. Barsoum, Nonlinear elastic deformation of MAX phases, Key Eng. Mater. 434–435 (2010) 149–153.
- [41] G.P. Bei, G. Laplanche, V. Gauthier-Brunet, J. Bonneville, S. Dubois, Compressive behavior of Ti₃AlC₂ and Ti₃Al_{0.8}Sn_{0.2}C₂ MAX phases at room temperature,

- J. Am. Ceram. Soc. 96 (2) (2013) 567-576.
- [42] A.G. Zhou, S. Basu, G. Friedman, P. Finkel, O. Yeheskel, M.W. Barsoum, Hysteresis in kinking nonlinear elastic solids and the Preisach-Mayergoyz model, Phys. Rev. B Condens. Matter Mater. Phys. 82 (9) (2010) 094105.
- [43] N.G. Jones, C. Humphrey, L.D. Connor, O. Wilhelmsson, L. Hultman, H.J. Stone, F. Giuliani, W.J. Clegg, On the relevance of kinking to reversible hysteresis in MAX phases, Acta Mater. 69 (2014) 149–161.
- [44] M.W. Barsoum, T. Zhen, A. Zhou, S. Basu, S.R. Kalidindi, Microscale modeling of kinking nonlinear elastic solids, Phys. Rev. B 71 (13) (2005) 1–8.
- [45] S.R. Kalidindi, T. Zhen, M.W. Barsoum, Macroscale constitutive modeling of kinking nonlinear elastic solids, Mater. Sci. Eng. A 418 (1–2) (2006) 95–98.
- [46] A.D. Kothalkar, R. Benitez, L. Hu, M. Radovic, I. Karaman, Thermo-mechanical response and damping behavior of shape memory alloy-MAX phase composites, Metallurgical Mater. Trans. A 45 (5) (2014) 1–13.
- [47] M.W. Barsoum, T. Zhen, S.R. Kalidindi, M. Radovic, A. Murugaiah, Fully reversible, dislocation-based compressive deformation of Ti3SiC₂ to 1 GPa, Nat. Mater. 2 (2) (2003) 107–111.
- [48] T. Zhen, M.W. Barsoum, S.R. Kalidindi, Effects of temperature, strain rate and grain size on the compressive properties of Ti₃SiC₂, Acta Mater. 53 (15) (2005) 4163–4171.
- [49] J.W. Hutchinson, Elastic- plastic behavior of polycrystalline metals and composites, Proc. R. Soc. A 319 (1537) (1970) 247–272.
- [50] P. Turner, C. Tomé, C. Woo, Self-consistent modelling of nonlinear viscoelastic polycrystals: an approximate scheme, Philos. Mag. A 70 (4) (1994) 689-711.
- [51] P.A. Turner, C.N. Tomé, A study of residual stresses in Zircaloy-2 with rod texture, Acta Metallurgica Materialia 42 (12) (1994) 4143–4153.
- [52] M. Barsoum, G. Tucker, Deformation of layered solids: ripplocations not basal dislocations, Scr. Mater. 139 (2017) 166–172.
- [53] J. Griggs, A.C. Lang, J. Gruber, G. Tucker, M. Taheri, M. Barsoum, Spherical nanoindentation, modeling and transmission electron microscopy evidence for ripplocations in Ti₃SiC₂, Acta Mater. 131 (2017) 141–155.
- [54] R. Benitez, W.H. Kan, H. Gao, M. O'Neal, G. Proust, M. Radovic, Room temperature stress-strain hysteresis in Ti₂AlC revisited, Acta Mater. 105 (2016) 294–305
- [55] M. Shamma, N.C. El'ad, B. Anasori, B. Clausen, D.W. Brown, S.C. Vogel, V. Presser, S. Amini, O. Yeheskel, M.W. Barsoum, In situ neutron diffraction evidence for fully reversible dislocation motion in highly textured polycrystalline Ti₂AlC samples, Acta Mater. 98 (2015) 51–63.
- [56] L. Hu, R. Benitez, S. Basu, I. Karaman, M. Radovic, Processing and characterization of porous Ti₂AlC with controlled porosity and pore size, Acta Mater. 60 (18) (2012) 6266–6277.
- [57] P. Gudlur, A. Forness, J. Lentz, M. Radovic, A. Muliana, Thermal and mechanical properties of Al/Al₂O₃ composites at elevated temperatures, Mater. Sci. Eng. A 531 (2012) 18–27.
- [58] M.W. Barsoum, T. El-Raghy, Room-temperature, ductile carbides, Metallurgical Mater. Trans. A 30 (2) (1999) 363–369.
- [59] N.V. Tzenvo, M.W. Barsoum, Synthesis and characterization of Ti₃AlC2, J. Am. Ceram. Soc. 83 (4) (2000) 825–832.
- [60] D. Chen, K. Shirato, M.W. Barsoum, T. El-Raghy, R.O. Ritchie, Cyclic fatigue-crack growth and fracture properties in Ti3SiC2 ceramics at elevated temperatures, J. Am. Ceram. Soc. 84 (3–12) (2001) 2914–2920.
- [61] M.H. Yoo, C.L. Fu, Physical constants, deformation twinning, and microcracking of titanium aluminides, Metallurgical Mater. Trans. A 29 (1) (1998) 49–63
- [62] S. Shu, B. Xing, F. Qiu, S. Jin, Q. Jiang, Comparative study of the compression properties of TiAl matrix composites reinforced with nano-TiB₂ and nano-Ti₅Si₃ particles, Mater. Sci. Eng. A 560 (2013) 596–600.
- [63] G.P. Bei, A. Guitton, A. Joulain, V. Brunet, S. Dubois, L. Thilly, C. Tromas, Pressure-enforced plasticity in MAX phases: from single grain to polycrystal investigation, Philos. Mag. 93 (15) (2013) 1784–1801.
- [64] J.A. Pelleg, Mechanical Properties of Ceramics, Springer, Cham Switzerland, 2014.
- [65] T.H. Courtney, Mechanical Behavior of Materials, McGraw Hill, Boston, USA, 2000.
- [66] J.B. Wachtman, W.R. Cannon, M.J. Matthewson, Dislocations and Plastic Deformation in Ductile Crystals, Mechanical Properties of Ceramics, John Wiley & Sons, Inc.,, Hoboken, NJ, USA, 2009.
- [67] M.A. Meyers, K.K. Chawla, Mechanical Behavior of Materials, Cambridge University Press, Cambridge, UK, 2009.
- [68] A. Guitton, S. Van Petegem, C. Tromas, A. Joulain, H. Van Swygenhoven, L. Thilly, Effect of microstructure anisotropy on the deformation of MAX polycrystals studied by in-situ compression combined with neutron diffraction, Appl. Phys. Lett. 104 (24) (2014) 241910.
- [69] N.J. Petch, The cleavage strength of polycrystals, J. Iron Steel Inst. 174 (1953) 25–28.
- [70] E.O. Hall, The deformation and ageing of mild steel: III Discussion of results, Proc. Phys. Soc. B 64 (9) (1951) 747–753.
- [71] N.J. Petch, Metallographic aspects of fracture, Fracture 173 (1968) 376–420.
- [72] M.F. Ashby, Deformation of plastically non-homogeneous materials, Phylosophical Mag. A 21 (170) (1970) 399–424.
- [73] M.A. Meyers, E. Ashworth, Model for the effect of grain size on the yield stress of metals, Philos. Mag. A 46 (5) (1982) 737–759.
- [74] E. Orowan, A type of plastic deformation new in metals, Nature 149 (3788) (1942) 643–644.

- [75] F.C. Frank, A.N. Stroh, On the theory of kinking, Proc. Phys. Soc. B 65 (10) (1952) 811–821.
- [76] M.W. Barsoum, M. Radovic, T. Zhen, P. Finkel, S.R. Kalidindi, Dynamic elastic hysteretic solids and dislocations, Phys. Rev. Lett. 94 (8) (2005) 1–4.
- [77] C. Zener, The Macro-mechanism of Fracture in Fracturing of Metals, American Society of Metals, Metalks Park, USA, 1948, pp. 3–31.
- [78] A. Stroh, The formation of cracks in plastic flow. II, Proc. R. Soc. A 232 (1191) (1955) 548–560.
- [79] A. Stroh, The formation of cracks as a result of plastic flow, Proc. R. Soc. A 223 (1154) (1954) 404–414.
- [80] R.W. Davidge, Mechanical Behaviour of Ceramics, Cambridge University Press, Cambridge, UK, 1979.
- [81] M. Radovic, M. Barsoum, A. Ganguly, T. Zhen, P. Finkel, S. Kalidindi, E. Lara-Curzio, On the elastic properties and mechanical damping of Ti₃SiC₂, Ti₃GeC₂, Ti₃Si_{0.5}Al_{0.5}C₂ and Ti₂AlC in the 300-1573 K temperature range, Acta mater. 54 (10) (2006) 2757–2767.
- 153:0,54:0,5€2 and 162AC in the 300-1573 K temperature range, Acta mater.
 54 (10) (2006) 2757-2767.
 [82] T. Liao, J. Wang, Y. Zhou, Deformation modes and ideal strengths of ternary layered Ti₂AlC and T_{i2}AlN from first-principles calculations, Phys. Rev. B 73 (21) (2006) 214109.